Innovative Infrastructure Solutions (2023) 8:293
https://doi.org/10.1007/s41062-023-01256-w

PRACTICE-ORIENTED PAPER

Differential scanning calorimetry of aluminium EN AB-42000 alloy rheocasting semi-solid in different stage heating rates

Kawan M. Abdulrahman[1,2] · Viktor Gonda[3] · Mihály Réger[3]

Received: 24 June 2023 / Accepted: 19 September 2023 / Published online: 17 October 2023

Abstract

Differential scanning calorimetry (DSC) is used to identify the thermal histories of samples to analyse and diagnose production and quality concerns connected to industrial rheocasting semi-solid alloy, that had undergone different tempers of aluminium alloy EN AB-42000 alloy. In this study, the solidus temperatures of several alloy samples are investigated using thermodynamic calculations and DSC observations in this work. The balance of important characteristics, including pseudo-eutectic, thermal sensitivity, heat flow, and enthalpies behaviour, of Al alloys has been investigated using experimental data from DSC and solid fractions. In addition, the choice of heating rates is critical as high rates can blur the two peaks in the mushy zone, while low rates lead to slower measurements. Using smaller sample weights and slower rates is preferable to obtain more accurate results. Analysing the shape of the *fs* curve, exact composition, and a reference composition without contaminants is essential for understanding complex behaviours, including pseudo-eutectic phenomena. The thermal sensitivity of compositions also plays a crucial role in the analysis. Despite heat flow decreasing with decreased sample weight, the measurement limit can still be exceeded at high heating or cooling rates (20 °C/min) during the eutectic reaction. The eutectic reaction exhibits higher peaks with enthalpies ranging from 360 to 430 mJ/g. However, drawing conclusions regarding trends in heating versus cooling or comparing low-mass and higher-mass samples can be challenging. The non-equilibrium transformation of the eutectic occurs within a more confined temperature range. Increasing rates lead to overlapping reactions, resulting in complex thermal behaviour.

Keywords Semi-solid · Rheocasting · Aluminium alloy EN AB-42000 · Differential scanning calorimetry (DSC) · Solid fraction

Introduction

Gently heating or cooling both a sample and a reference chamber, differential scanning calorimetry (DSC) measures the difference in heat flow between the two chambers. By subjecting the sample and reference to controlled temperature changes, DSC enables the characterization of thermal properties and processes of the material under investigation. This technique provides insights into phase transitions, reactions, melting points, and other thermal phenomena by comparing the heat flow of the sample to that of the reference. DSC is a versatile and widely used analytical tool in materials science, chemistry, and other fields [1]. An adiabatic insulator separates the two chambers. The molecule of interest is contained in a suitable buffer in the sample chamber, whereas the reference chamber has the same buffer [2]. The Al-Si system's phase diagram appears to be rather straightforward [3]. Even at temperatures significantly lower

✉ Kawan M. Abdulrahman
kawan.abdulrahman@bgk.uni-obuda.hu

Viktor Gonda
gonda.viktor@bgk.uni-obuda.hu

Mihály Réger
reger.mihaly@bgk.uni-obuda.hu

[1] Doctoral School on Materials Sciences and Technologies, Óbuda University, Budapest, Hungary

[2] Department of Mechanical and Manufacturing Engineering, College of Engineering, Sulaimani Polytechnic University, Sulaimani, Kurdistan, Iraq

[3] Bánki Faculty of Mechanical and Safety Engineering, Óbuda University, Budapest, Hungary

than the thermal unfolding or "melting" temperature (Tm), there is still a noticeable disparity in heat flow between the sample cell and the reference cell when the sample contains a protein [4]. This disparity occurs because energy is supplied to the protein, leading to the disruption of non-covalent interactions that maintain its solvation, secondary, and tertiary structures. As a result, more heat flows into the sample cell compared to the reference cell, reflecting the energy input required to modify the protein's structural arrangements. This observation highlights the sensitivity of differential scanning calorimetry (DSC) in detecting even subtle changes in protein conformation and behaviour at temperatures below the Tm. [5]. In the DSC process, as the temperature gradually rises, there comes a point where the protein initiates its unfolding. At this stage, there is a noticeable and substantial increase in the disparity of heat flow between the sample and reference chambers. This increase reaches its peak at a specific temperature known as Tm, which represents the midpoint of the unfolding process [6]. Subsequently, as the unfolding process is finalized, the heat flow begins to decline, leading to a distinct peak in the plot of heat flow versus temperature, also known as a thermogram. This thermogram provides valuable information about the unfolding characteristics and thermal stability of the protein under investigation. [7].

A popular casting method for creating components made of aluminium is called Al semi-solid rheocasting. In this procedure, an aluminium slurry is created utilizing methods like mechanical stirring or electromagnetic stirring [8]. The automotive and aerospace industries extensively employ the Al semi-solid rheocasting process to manufacture engine blocks, suspension parts, wheels, and other components [9]. This technology provides precise dimensional control, reduced porosity, and improved surface finish, making it a favourable option for aluminium component manufacturing. Overall, the Al semi-solid rheocasting process offers a cost-effective and eco-friendly approach to producing high-quality, complex-shaped aluminium components compared to conventional casting methods [10].

The novel DSC technique proves to be highly beneficial in commercial applications of AA6xxx alloys. These alloys are now supplied in pre-aged conditions, offering enhanced technical qualities [11]. In this context, DSC plays a crucial role in optimizing both the processing techniques and the material properties. By analysing the heat flow and thermal behaviour of the alloys, DSC allows for a thorough understanding of the ageing process and helps fine-tune the processing parameters. This optimization leads to improved control over the final properties of the AA6xxx alloys, making the DSC technique a valuable tool in the industry [12].

The first endothermic peak's enthalpy grew, whereas the second endothermic peak's enthalpy dropped with an increase in silicon concentration. For powders without silicon addition, an endothermic peak was seen, while in the case of alloys with Si addition, it was conspicuously lacking [13].

The importance and implications of key characteristics are typically investigated in a differential scanning calorimetry (DSC) analysis of an aluminium alloy like EN AB-42000. These characteristics include pseudo-eutectic behaviour, thermal sensitivity, heat flow, and enthalpy changes [14].

Pseudoeutectic behaviour provides crucial insights into the alloy's solidification behaviour and its resulting microstructure, influencing how the material is used and processed. Thermal sensitivity, determined through shifts and changes in peak shape or size in DSC analysis, can offer an understanding of the alloy's behaviour under various temperatures, essential in many applications that require varying temperatures or swift temperature changes [15].

The heating rate can significantly affect the outcomes of the DSC analysis. It can cause shifts in the temperature at which phase transformations occur, resulting in peak broadening that reduces the resolution of different events, and influences the emphasis on kinetic effects, with slow and fast heating rates producing different results [16].

The heating rate also affects observations in the "mushy zone" (temperature range where the alloy is partly solid and partly liquid) which is critical to the rheocasting process. Faster heating rates can cause the mushy zone to appear narrower and shift to higher temperatures [17].

Standard scan speeds irrelevant for industrial applications are frequently used in DSC studies for solid fraction analysis [18]. The relationship between the solid percentage and temperature is of utmost importance for experimental assessment and mathematical modelling purposes. Understanding how the solid percentage changes with temperature provides valuable insights into the behaviour and characteristics of the material under study [19]. This relationship forms the foundation for developing accurate mathematical models that can predict and simulate the material's response to temperature variations. Experimental assessment coupled with mathematical modelling utilizing this relationship enables researchers to gain a comprehensive understanding of the material’s properties, allowing for better analysis, optimization, and design of various processes and systems [20].

In this work, we conducted a detailed analysis using thermodynamic calculations and differential scanning calorimetry (DSC) data to study the solidus temperatures of various EN AB-42000 rheocasting semi-solid samples, considering changes in sample dimensions. Furthermore, based on DSC experimental data and solid fractions, we examined the EN AB-42000 rheocasting semi-solid alloys. Specifically, we studied the balance of critical properties, including pseudo-eutectic, thermal sensitivity, heat flow, and enthalpies behavior. In addition, all processes are a series of heating include,

determining two-stage heating rates alloy to 550 °C; fast then slow heating alloy, fast cooling alloy, fast heating alloy to 600 °C, quick alloy heating to 650 °C and cooling not important, rapid alloy heating to 700 °C, controllable heating alloy to 700 °C; fast alloy heating to 700 °C, controllable heating alloy to 700 °C; quick alloy heating to 700 °C, controllable heating alloy to 700 °C; rapid alloy heating to 700 °C The quantity varies due to different precipitation patterns. Solid fractions were determined similarly by cycling temperatures between 500 and 700 °C at different rates (0.5, 1, 2, 5, 10, and 20 °C/min), recording heating and cooling, and computing solid fractions.

Metal and methodology

Table 1 shows the chemical compositions of the alloys utilized in this study. The aluminium silicon alloy grade (EN AB-AlSi7) is commonly used for pressure-tight castings that are susceptible to fatigue loading. After heat treatment, it has good corrosion resistance and high strength [21, 22].

The aluminium alloy EN AB-42000 is an alloy in the wrought Al-Si series 4xxx, which is not strongly included in ASTM standards. Aluminium alloy EN AB-42000 is generally formed by rolling and extrusion. Despite its uncommon practice with this alloy, the series can also be forged and clad [23]. The main applications are scaffolding automotive, aerospace, electronics elements, rail coach parts, offshore constructions, containers, machine-building, and mobile cranes [23]. Using alloy EN AB-42000 in the above applications displays good resistance to dynamic loading conditions. The resistance is attributed to its fine-grained structure. Besides this alloy, EN AB-42000 is an expert in marine applications [24]. In the practical alloy EN AW 4244, the aluminium alloy contains Si in a 6.5–7.5 wt% range. This alloy typically has more than one type of Si and exhibits unique properties at semi-solid temperatures [25]. When searching for its ASTM counterpart, it is essential to examine the unique chemical makeup and mechanical attributes of EN AB(AC)-42000, aiming to identify an ASTM B518 alloy with similar properties.

Rheocasting has been known as such since ground-breaking research at MIT in 1972 when it was discovered that metals in the semi-solid state, with globular grains, exhibit unique rheological characteristics that make them appropriate for high-quality component casting [26].

Over the years, numerous techniques have been developed to create semi-solid slurries for rheocasting. One crucial aspect of this process is to prevent the formation of dendritic grains when transitioning a liquid into a semi-solid state. To achieve this, it is essential to have precise control over the heat extraction while simultaneously employing vigorous stirring or similar mechanisms. This combination of controlled cooling and intense agitation helps ensure the formation of uniform, fine-grained slurries suitable for rheocasting [27]. By carefully managing these parameters, manufacturers can optimize the rheocasting process and produce high-quality components with desirable microstructures and mechanical properties [28]. A slurry with tiny, spherical grains and a well-controlled solid fraction should result. In addition, the process should be able to create huge volumes of slurry in a short length of time at a low cost. Unfortunately, most methods have failed to meet at least one of these criteria, which is why rheocasting is still a niche industry [29].

Result and discussion

The Al semi-solid rheocasting method is a widely adopted casting process for producing aluminium-based components. This process involves the creation of a semi-solid slurry of aluminium using techniques like mechanical stirring or electromagnetic stirring. The semi-solid slurry is then processed using a die-casting method, where it is injected into a die cavity to achieve the desired shape. Compared to traditional casting methods, this process yields materials with enhanced mechanical properties, including improved hardness, low porosity, and superior surface finish [30].

Differential scanning calorimetry (DSC) is a widely used analytical technique in materials science and chemistry. It measures the heat flow into or out of a sample as a function of temperature or time. DSC works by comparing the heat flow of a sample to that of a reference material as they both undergo controlled temperature changes [31].

The significance of the solidus temperature—a crucial parameter in the rheocasting process—and the methods employed for its determination, namely thermodynamic calculations and differential scanning calorimetry (DSC). Both methods come with their own set of challenges and considerations [32].

Thermodynamic calculations use software tools to predict the solidus temperature based on the alloy's composition and each component's thermodynamic properties. However, the accuracy of these calculations relies heavily on the quality of the underlying database, and they assume that the

Table 1 The chemical composition of Aluminium EN AB-42000 alloys

wt%	Al	Mg	Si	Sn	Fe	Mn	Cu	Ti	Zn	Pb	Ni
EN AB-42000	Bal	0.25	6.5–7.5	0.05	0.45	0.35	0.15	0.20	0.15	0.15	0.15

alloy is at thermodynamic equilibrium, which may not be true in real-world conditions. DSC, on the other hand, is an experimental technique that measures the heat absorbed or released by a sample during heating or cooling. This method can directly determine the solidus temperature. However, its accuracy can be affected by factors such as the sample's size and homogeneity, the heating rate, and the calibration of the DSC instrument itself.

By using both methods in conjunction, a more accurate determination of the solidus temperature can be achieved, providing a more complete understanding of the alloy's behaviour [33].

Semi-solid rheocasting method

The EN AB-42000 alloy has a melting temperature of 680 °C. The phase diagram depicts the influence of AlSi7 weight per cent and phase transition temperatures [8]. The alloy was melted at 700 °C in an electric resistance furnace [10]. To allow for melting temperature, the alloy was kept in this furnace for minutes. The crucible was removed from the furnace, and the molten metal was placed in a stainless steel cylinder cup, which was permitted to cool at room temperature. The procedure outlined above was repeated for the same metal during the rheocasting process. Once the crucible was removed from the furnace, the melted metal was internally cooled using a 'K type' thermocouple to regulate the temperature. Subsequently, the molten metals were vigorously agitated for a few seconds at 640 °C using steel attached to a spinning electric hand drill. This agitation was performed until the melt completely dissolved, aiming to produce globular shapes and disrupt the dendritic structure. To prevent dendritic growth, the alloy should be cooled to room temperature with water as soon as the dendritic microstructure is replaced with a globular microstructure [30]. DSC has been used in several studies to investigate solid-state phenomena in aluminium alloys, such as precipitation and dissolution of precipitates, as well as precipitation kinetics during heat treatments [24]. The specimen under inquiry and a reference specimen is heated and cooled at the same time in a DSC experiment [34]. Within the examined temperature range, the reference specimen must not display any phase change [35]. During such a heating cycle, the difference in energy consumption or output per time and mass between the specimen and the reference is measured. As a function of temperature, this so-called heat flow is displayed. An exothermic process, such as solidification or precipitation, is indicated by a positive peak. An endothermic process, such as melting or dissolution, is represented as a negative peak [36]. The semi-solid rheocasting offers several advantages over conventional casting techniques, making it especially suitable for aluminium alloys like EN AB-42000. These benefits include improved flow ability, reduced defects (like porosity and hot tearing), enhanced mechanical properties, and lower energy consumption. Furthermore, rheocasting is cost-efficient, producing near-net-shape parts requiring less machining. These advantages enhance the performance and viability of components made from EN AB-42000, a widely used alloy in demanding sectors like automotive, aerospace, and electronics industries [37]. Further details can be found in the authors previous studies [33].

DSC samples used in dimensions and crucible type

The rheocasting can offer additional and valuable insights into the solidus temperature of an alloy, which can complement or enhance the information obtained from traditional techniques like thermodynamic calculations or differential scanning calorimetry (DSC) analysis. The advantages of rheocasting include its ability to reflect real-world conditions, its use of larger, more representative samples, the possibility of visual observation, and the opportunity for post-process microstructure analysis. However, rheocasting is not a replacement for other methods but should be used in conjunction with them to obtain a comprehensive understanding of an alloy's behaviour.

Smaller sample sizes are preferred for DSC measurements to ensure even heating throughout the sample and a quicker response to changes in temperature. Larger, non-homogeneous samples may heat unevenly, and their thermal inertia might slow down responses to temperature changes, leading to inaccurate results.

Similarly, slower heating rates are advantageous as they allow sufficient time for phase transformations to occur at their "proper" temperatures. Faster heating rates may cause these transformations to appear at higher temperatures and can also reduce the resolution of closely spaced thermal events.

The use of smaller sample weights and slower heating rates can lead to sharper, better-defined peaks in the DSC curve and a more accurate determination of phase transition temperatures. This improves the understanding of the alloy's thermal behaviour and makes it easier to interpret different thermal events. As a result, this approach can provide valuable insights for optimizing processes like rheocasting. Table 2 shows the number of DSC tests, including samples, measurements of alloy tape, sample dimension, and crucible type utilized in the test.

Heating vs cooling: Differences can arise due to thermal hysteresis and kinetic effects. Interpretation of these differences can be complex, particularly if more energy is required to melt the alloy than is released during solidification.

Low-mass vs higher-mass samples: Issues with heat transfer, differences in microstructure, and sample representativeness could all affect the observed thermal behaviour.

Table 2 DSC dimension of samples, crucible type, and sample preparations

Samples	measurements	Tape of alloy	Dimension of the sample			Crucible-type ceramic mg	Sample preparation
			Diameter mm	High mm	Wight gm		
1	1	$AlSi_7$ Rheocasting semi-solid	4.5	3	124.7	152.3	–
	2						
	3						
	4						
	5						
2	6				116.5		
	7						
3	8				120.3	153.3	
	9				83.1	152.3	
	10					153.3	
	11						Rinse in ethanol, wipe with a paper towel
4	12		4.5	2	83.1	152.3	Clean in ethanol, wipe with a paper towel
5	13		4.5	1	40.1	153.5	

To gain more accurate insights, researchers can mitigate these challenges by conducting multiple experimental runs, utilizing complementary characterization techniques, and applying theoretical calculations.

DSC heating curve of the Al alloy measured heat flow two-stage heating rates to 550 °C; fast then slow heating; fast cooling

The measurement sample was two-stage heating rates to 550 °C and fast then slow heating, in the second stage fast cooling sample. The thermal cycle for the first measurement started heating to 500 °C at 100 °C/min, heating to 550 °C at 50 °C/min, holding at 550 °C for 1 min, and cooling to RT at 100 °C/min.

In Fig. 1a, the analysis measurement of the sample is displayed. We can observe a small exo peak around 350 °C and a sudden drop in heat flow at 500 °C when there's a change in the heat rate. Control stabilises as the range increases by about 20 °C, and rapid cooling ensues. However, control is lost at 350 °C, making the cooling rate of 100 °C/min unsuitable for results and sample inspection. Notably, no melting occurs in this instance.

Conversely, Fig. 1b provides an analysis measurement where the small exo peak at around 350 °C is absent. The endo-reaction begins at approximately 570 °C, suggesting potential melting. During cooling, a prominent exo peak indicates solidification. A cooling rate of 50 °C/min is applicable for this measurement. Upon sample inspection, there was a noticeable color change, indicating that some melting might have taken place. The sample did not stick to the holder. The second measurement of the first sample was fast heating to 600 °C. The thermal cycle for the second measurement started heating to 600 °C at 50 °C/min, heating

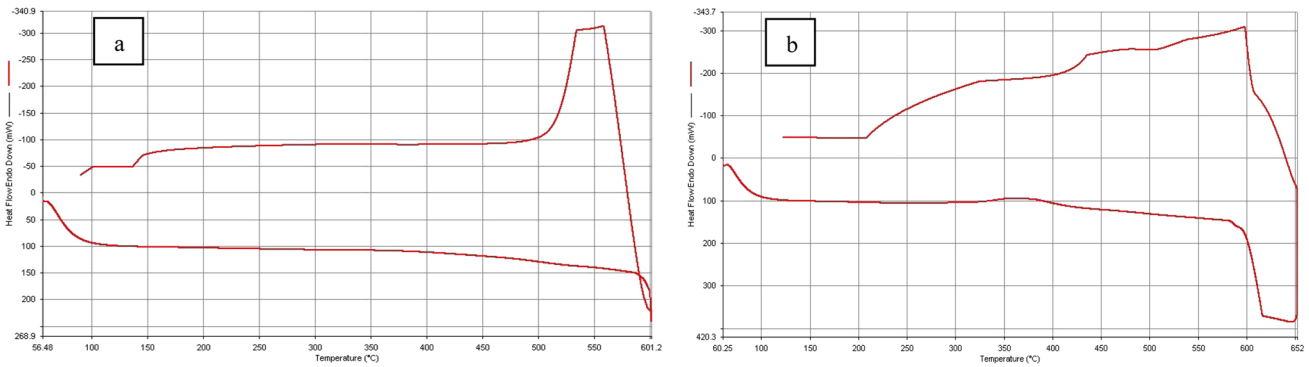

Fig. 1 **a** DSC heating curves of the Al alloy first Sample Measured heat flow 2-stage heating rates to 550 °C; fast then slow heating; fast cooling, **b** heat flow fast heating to 600 °C

to 600 °C at 50 °C/min, holding at 600 °C for 1 min, and cooling to RT at 50 °C/min.

In a DSC analysis, when the heating or cooling rates are high (for instance, 20 °C/min), the rapid energy changes that occur during phase transformations might exceed the measurement limit of the DSC instrument. This limitation can lead to inaccurate enthalpy measurements, difficulty in distinguishing thermal events, and potential misinterpretation of the alloy's thermal behaviour. Several steps can be taken to mitigate these limitations: reducing the heating or cooling rate can result in more accurate measurements; using smaller samples can decrease the total energy change, reducing the likelihood of exceeding the measurement limit; using a high-capacity DSC instrument with higher measurement limits can handle larger heat flows.

The heating curve of Al alloy measured heat flow up to 650 °C and 700 °C, while cooling wasn't significant

The measurement of the sample was fast heating to 650 °C and cooling was not important. The thermal cycle for the third measurement started heating to 650 °C at 50 °C/min, holding at 650 °C for 1 min, and cooling to RT at 100 °C/min.

Figure 2a shows an analysis third measurement of the first sample was a small exo peak at around 350 °C, endo-reaction starts at about 570 °C, with a small peak, then a large one. Melting might not be completed, a cooling rate too high, not measurable, and sample inspection; colour changed, some melting might occur. The sample did not stick to the holder.

Figure 2b demonstrates an analysis measurement of the sample where a small exo peak at around 350 °C, endo reaction onset at around 570 °C, with a small peak, then a large one, large, elongated peak-end at about 670 °C, complete melting captured, a cooling rate too high, not measurable and sample inspection; colour changed, some melting might occur. The piece did not stick to the holder.

The fourth measurement of the first sample was fast heating to 700 °C. The thermal cycle for the fourth measurement started heating to 700 °C at 50 °C/min, holding at 700 °C for 1 min, and cooling to RT at 100 °C/min.

DSC heating curves of the Al alloy measured heat flow-controlled heating to 700 °C

The measurement of the sample aimed to control heating to 700 °C. The thermal cycle for the fifth measurement started heating to 700 °C at 20 °C/min, holding at 700 °C for 1 min, and cooling to RT at 100 °C/min.

Figure 3a and b illustrates the analysis measurements of the sample. A small Exo peak appears at around 350 °C, followed by an endo reaction onset at approximately 570 °C. This is initially marked by a small peak, which then escalates to a more significant peak ending around 650 °C, indicating complete melting. Due to the excessively high cooling rate, the measurement couldn't be taken. Upon inspecting the sample, a change in color was observed, suggesting that some melting might have occurred. The sample did not stick to the holder.

Heating curve of Al alloy measured controlled heating and cooling cycles at 700 °C with slow heat flow

The measurement of the sample aimed to control heating to 700 °C, and control cooling; repeated cycle. The thermal cycle for the sixth measurement started heating to 700 C at 20 °C/min, holding at 700 °C for 1 min, cooling to 300 at 40 °C/min, holding at 300 °C for 1 min, heating to 700 °C at 20 °C/min, hold at 700 °C for 1 min and cooling to RT at 40 °C/min.

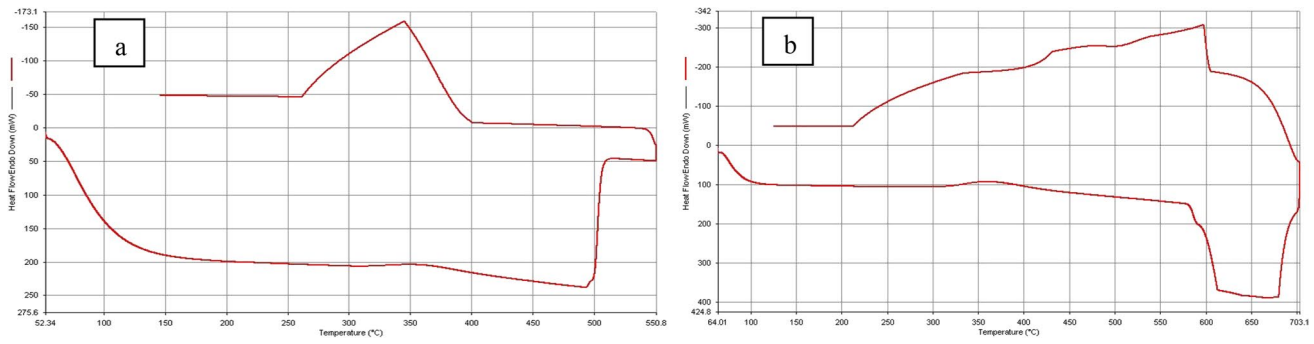

Fig. 2 **a** DSC heating curves of the Al alloy third Sample Measured heat flow fast heating to 650 C, **b** cooling is not important and heat flow fast heating to 700 °C

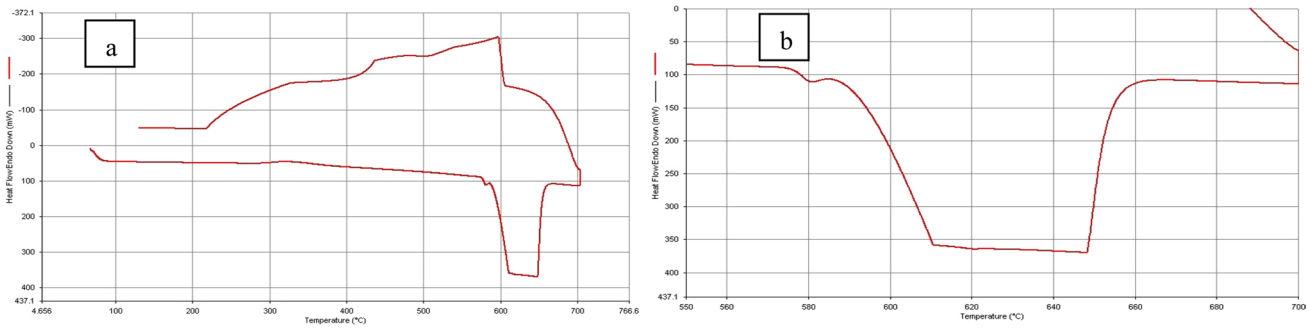

Fig. 3 **a** DSC heating curves of the Al alloy fifth Sample Measured heat flow-controlled heating to 700 °C at 20 °C/min and hold at 700 °C for 1 min, **b** cooling to RT at 100 °C/min

Figure 4a Figure 4a illustrates the analysis measurement of the sample. The results indicate that complete melting occurred, and the cooling rate was deemed satisfactory.

Measured elongated exo peak during solidification onset just below 620 °C; a small endo peak at the middle, sample inspection, the colour changed, some melting might occur, and the sample did not stick to holder.

Figure 4b presents the analysis measurement of the sample. At the observed rate, we can identify 2 distinct peaks. The onset of the endo reaction starts around 570 °C, marked by a minor peak. This is followed by a more prominent peak indicating initial melting. A subsequent peak, culminating at about 650 °C, signifies complete melting. The cooling rate was found to be satisfactory.

Measured elongated exo peak during solidification onset at 630 °C; a second peak ended at 565 °C, for heating. The liquid fraction is calculated by integrating the peaks. For cooling, the solid fraction is calculated by integrating the peaks, sample inspection: colour changed, some melting might occur, and the sample did not stick to the holder. The aim of the measurement of the sample was slow heating to 700 °C and slow cooling; repeated cycle. The thermal cycle for the seventh measurement started heating to 700 °C at 5 °C/min, holding at 700 °C for 1 min, cooling to 300 at 5 °C/min, and cooling to RT.

The heating curve of the Al alloy measured measurement 8, multi-cycle

The aim of the eighth measurement of the third sample was cycling temperatures between 500 and 700 °C with different rates (0.5, 1, 2, 5, 10 and 20 °C/min), recording heating and cooling, calculating solid fractions

Figure 5 demonstrates an analysis measurement of the sample was heating and cooling, calculating solid fractions. In our analysis, we observed that the onset of melting occurs around 590 °C and has limited dependence on the heating rate. For each heating rate, heat flow curves consistently follow the same pattern. However, the conclusion of the melting process is strongly tied to the heating rate, with peak heights rising correspondingly. Notably, at heating rates of 10 and 20 °C/min, the heat flow surpasses the measurable range. Additionally, a minor peak usually seen at 580 °C is absent at these rates. The cooling analysis cooling peaks shift to the left, the onset of solidification is dependent on the cooling rate, and the ending of solidification is highly

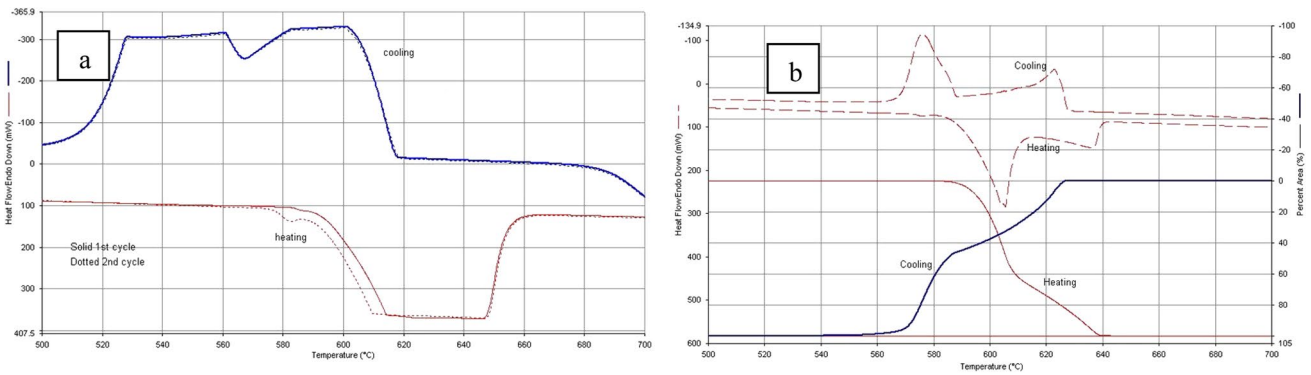

Fig. 4 **a** DSC heating curve of the Al alloy sixth Sample Measured heat flow-controlled heating to 700 °C, and controlled cooling; repeated cycle, **b** measured heat flow slow heating to 700 °C, and slow cooling

dependent on the cooling rate. Upon inspecting the specimen, a darkened surface with indications of melting was observed. The diameter appears to have increased, yet the specimen can still be removed from the holder.

Figures 6, 7, 8 demonstrate an analysis measurement of the sample was heated rates at 10 and 20 °C/min; peaks were smeared. High values exceeding measurement limits, at lower rates, 2 separated peaks for the eutectic reaction and complete melting temperatures, even at low rates, heating, and cooling peaks were shifted; repeated cycles show good measurement reliability.

The first heating/cooling and first reheat cycles at 0.5 °C/min show some minor deviation, indicating a difference between the initial state and the reheated state of the

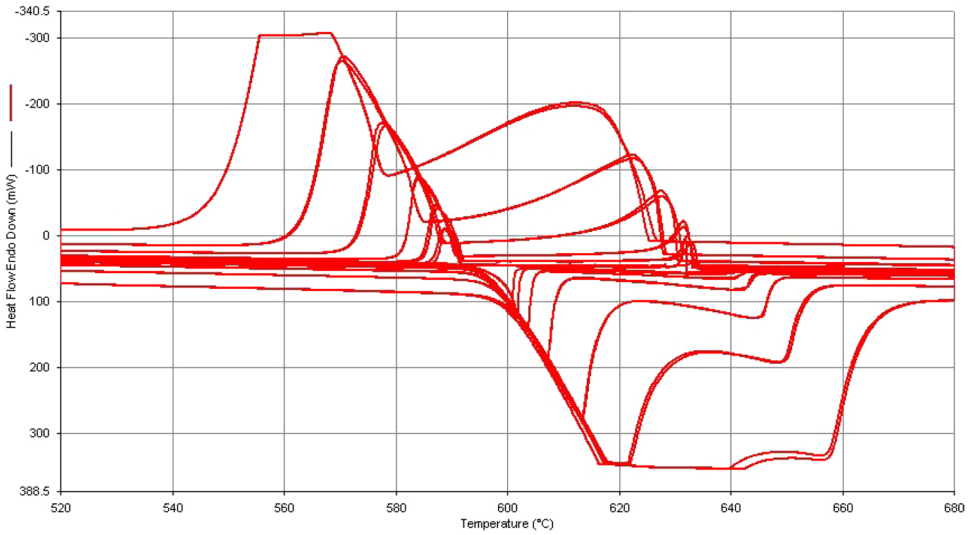

Fig. 5 DSC heating curve of the alloy eighth Sample measured heat flow overview, multi-cycle

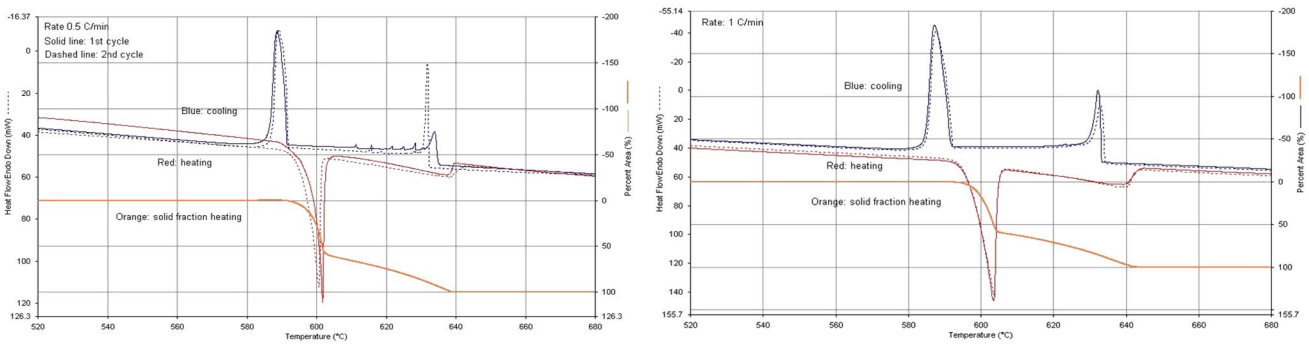

Fig. 6 DSC heating curve of the Al alloy Heating, cooling, and first cycle solid fraction for 0.5 °C/min and 1 °C/min heating rate

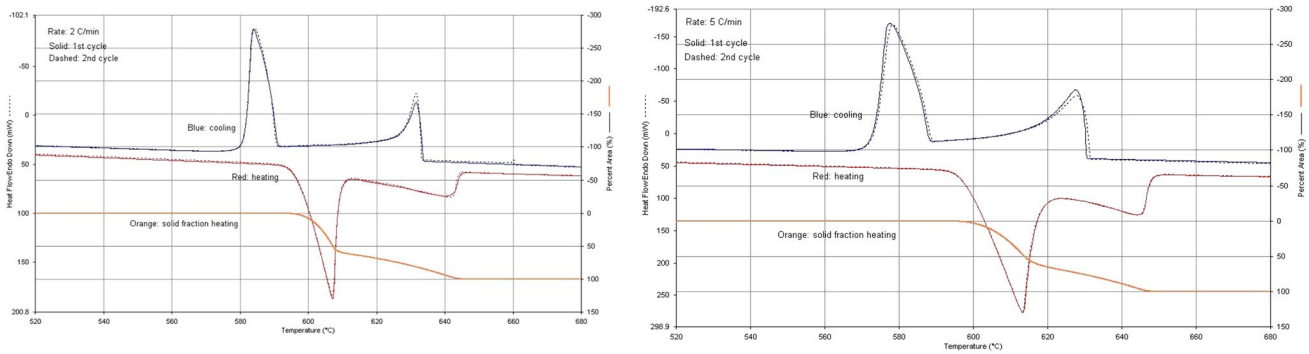

Fig. 7 DSC heating curve of the Al alloy Heating, cooling, and first cycle solid fraction for 2 °C/min and 5 °C/min heating rate

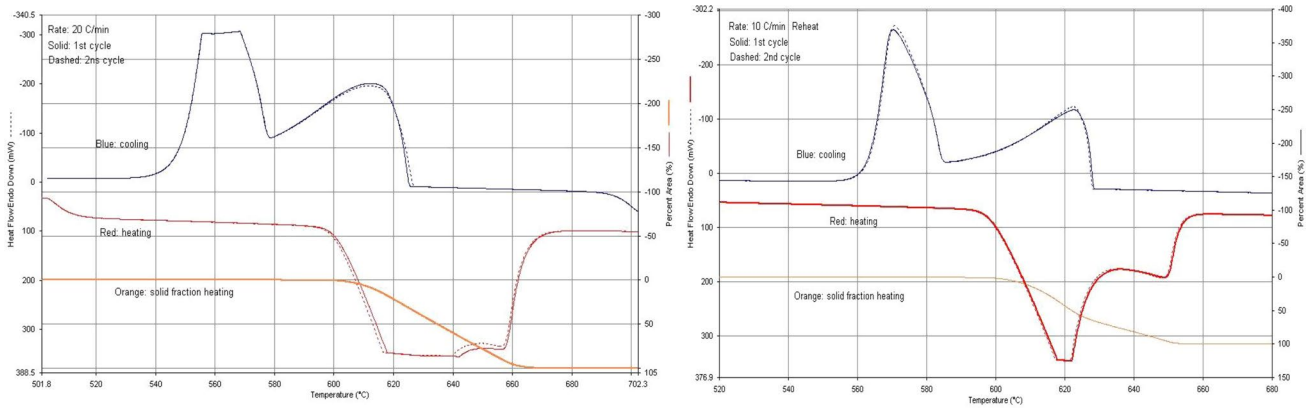

Fig. 8 DSC heating curve of the Al alloy Heating, cooling, and first cycle solid fraction for 10 °C/min and 20 °C/min heating rate

Table 3 Heat rate, Solid fraction transient temperatures, and energy in transformation extracted data

Rate (°C/min)	Solid fraction transient temperatures (C)			Energy in transformation (mJ)
	Onset	Break ($fs = 0.6$)	Ending	
0.5	590	602	638	45,350
1	592	603	642	45,785
2	591	610	645	46,003
5	595	615	648	47,340
10	595	625	653	45,635
20	598	–	668	40,506

sample, and there is a breakpoint in the solid fraction curves at about $fs = 60\%$. There is a significant difference between the S parameter ($S = df/dT$) S = 0.6/10 (1/°C) in the range of $fs = 0$–60%; and S = 0.4/40 (1/C) at $fs = 60$–100%.

Table 3 illustrates an analysis measurement of the sample where characteristic temperatures are the onset of the transformation, a break-point, and the ending. All temperatures show an increasing trend with the rising heating rates; partially from the physical fact of material behaviour, and partially from the thermal lag of the measurement method and the increase of the transformation energy (e.g. total latent heat) shows also an increase with the heating rate; a deviation was seen at 10 and 20 °C/min due to the exceeded measurement limit.

The *fs* curve represents the fraction of solid phases present in the alloy as a function of temperature during cooling, offering vital insights into the solidification process. It shows the temperatures at which solidification begins (liquids) and ends (solidus), marking the range known as the mushy zone where the alloy is semi-solid. Changes in the curve can indicate complex behaviours such as pseudo-eutectic reactions, wherein a solid phase and a liquid phase transform into a different solid phase of the eutectic composition.

The heating curve of Al alloy recorded rates of heating and cooling, calculating solid and liquid fractions

The aim of the measurement of the sample was cycling between 500 and 700 °C with different rates (0.5, 1, 2, 5, 10, 20 °C/min), recording heating and cooling, and calculating solid and liquid fractions. (Fig. 9) demonstrates a ninth analysis measurement of the third sample was heating and cooling, calculating solid fractions. In analysis, two peaks can be identified, the low-temperature peak is for the melting/solidification of the eutectic, and the high-temperature peak is for the melting/solidification of the alpha phase.

The two peaks may overlap depending on the heating and cooling rate. On heating rate, the onset of melting is less dependent, at about 590 °C; at each heating rate, heat flow curves follow the same envelope, ending of melting is highly dependent on the heating rate, Peak heights increase with the heating rate, at 10 °C/min and 20 °C/min heat flow exceeds the measurable range, tiny peak at 580 °C is missing. On cooling rate, cooling peaks shift to the left, the onset of solidification is dependent on the cooling rate, and ending of solidification is highly dependent on the cooling rate. Inspection of the specimen reveals darkened surface with signs of melting; the diameter might have been increased; nevertheless, the specimen can be taken out of the holder.

Figures 10, 11, 12 demonstrate an analysis measurement of the sample was heated rates at 10 and 20 °C/min, peaks are smeared, and high values exceeding measurement limits, at lower rates, two separated peaks for the eutectic reaction and complete melting temperatures.

The observed enthalpies during the differential scanning calorimetry (DSC) analysis of the aluminium alloy EN AB-42000 are within the range of 360–430 mJ/g. There are observable trends, but drawing firm conclusions from them is challenging due to the complexities of the system. Two key trends were observed:

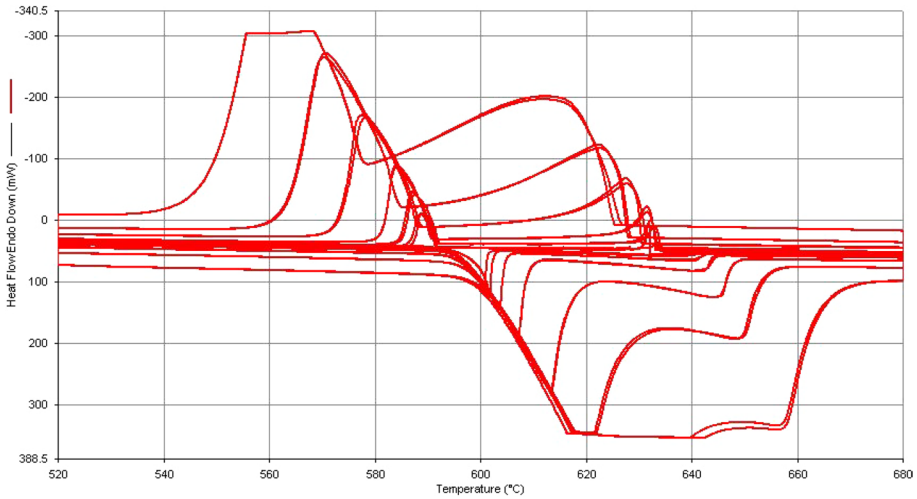

Fig. 9 DSC heating curve of the Al ninth Sample measured heat flow overview, multi-cycle cooling

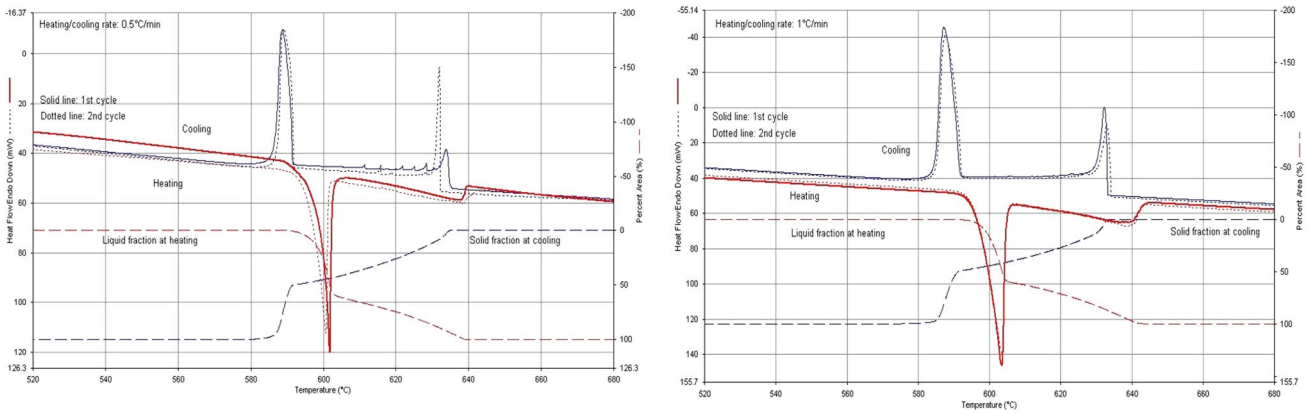

Fig. 10 DSC heating curve of the Al alloy Heating, cooling, and first cycle solid fraction for 0.5 °C/min and 1 °C/min heating rate

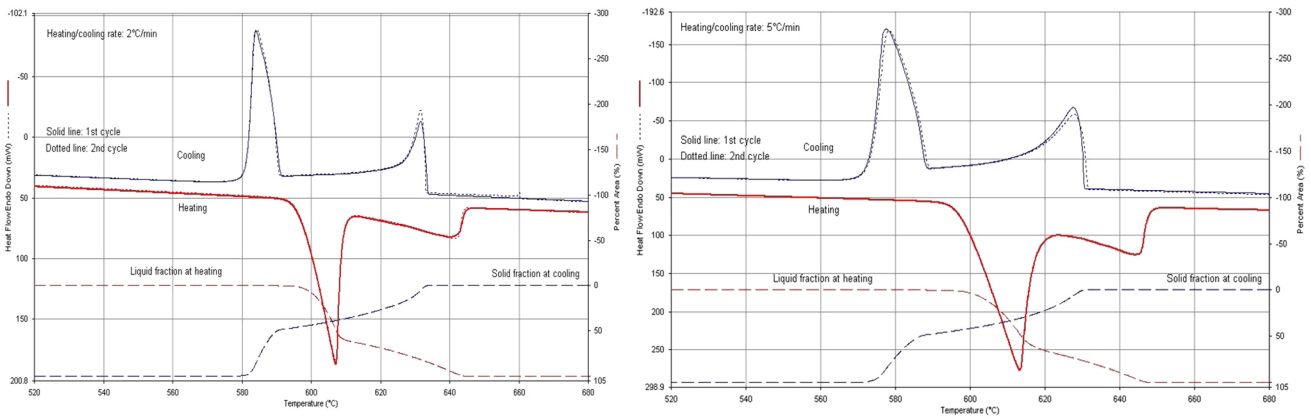

Fig. 11 DSC heating curve of the Al alloy Heating, cooling, and first cycle solid fraction for 2 °C/min and 5 °C/min heating rate

a. The enthalpy during the heating process might be higher than during cooling. This could be attributed to various factors, including the difference in energy requirements for phase transitions during heating and cooling, or possible kinetic and thermal hysteresis effects.

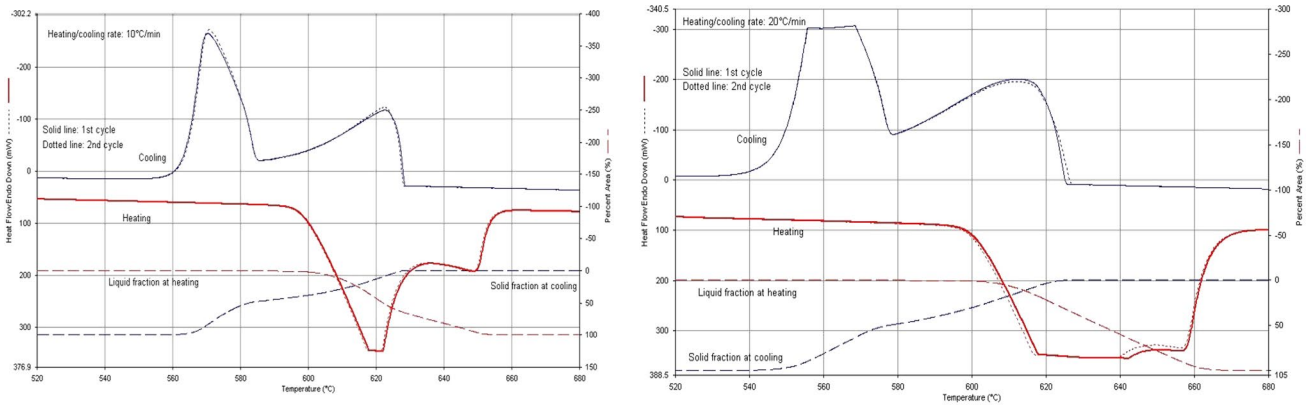

Fig. 12 DSC heating curve of the Al alloy Heating, cooling, and first cycle solid fraction for 10 °C/min and 20 °C/min heating rate

Table 4 Heat rate, solid fraction transient temperatures, and energy in transformation extracted data for heating rates

Heating rate (C/min)	Liquid fraction transient temperatures (C)			Energy in transformation (mJ)
	Onset	Break ($fl=0.6$)	Ending	
0.5	590	602	638	45,350
1	592	603	642	45,785
2	591	610	645	46,003
5	595	615	648	47,340
10	595	625*	653	45,635*
20	598	–*	668	40,506*

*Heat flow exceeds measurement limits

Table 5 Cooling rate, solid fraction transient temperatures, and energy in transformation extracted data for cooling rates

Cooling rate (C/min)	Solid fraction transient temperatures (C)			Energy in transformation (mJ)
	Ending	Break ($fs=0.5$)	Onset	
0.5	582	590	635	47,481
1	580	592	633	47,590
2	578	588	634	46,135
5	571	585	630	46,046
10	558	579	627	46,193
20	535	575	625	43,775*

*Heat flow exceeds measurement limits

b. The samples with lower mass tended to show higher enthalpies than those with a higher mass. This could be due to the more rapid attainment of thermal equilibrium in smaller samples, leading to more efficient heat absorption or release, or potentially due to differences in heat flow or microstructure.

Even at low rates, heating, and cooling peaks are shifted, and repeated cycles show good measurement reliability. The first heating/cooling and first reheat cycles at 0.5 °C/min show some minor deviation, indicating a difference between the initial state and the reheated state of the sample. There is a breakpoint in the liquid fraction curves at about $fl=60\%$. There is a significant difference between the S parameter ($S=df/dT$) S = 0.6/10 (1/°C) in the range of $fs=0$–60%; and S = 0.4/40 (1/°C) at $fs=60$–100%. The breakpoint at cooling is at $fs=50\%$.

Tables 4 and 5 illustrate an analysis measurement of the sample where characteristic temperatures are the onset of the transformation, a breakpoint, and the ending of the transformation.

Extracted data, at heating, all temperatures show an increasing trend with the rising heating rates: partially from the physical fact of material behaviour and partially from the thermal lag of the measurement method. The increase of the transformation energy (e.g. total latent heat) also shows an increase in the heating rate; a deviation is seen at 10 and 20 °C/min due to the exceeded measurement limit. Extracted data, at cooling, all temperatures show a decreasing trend with the increasing heating rates, partially from the physical fact of material behaviour and partially from the thermal lag of the measurement method. There is a decrease in the transformation energy with increasing cooling rates; the thermal capacity of the sample holder may cause a reduction in the apparent heat measured; a deviation is seen at 20 °C/min due to the exceeded measurement limit.

The heating curve of Al alloy recorded rates of heating and cooling, calculating solid and liquid fractions through multi-cycles with reduced mass

The aim of the measurement of the sample was cycling between 500 and 700 °C with different rates (0.5, 1, 2, 5,

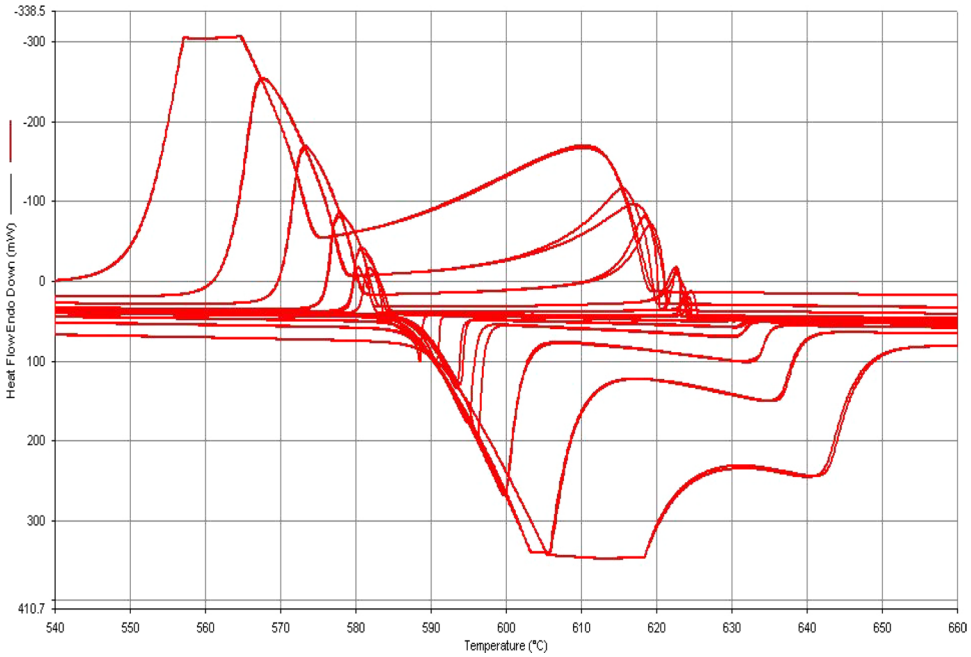

Fig. 13 DSC heating curve of the Al alloy tenth Sample measured heat flow overview, multi-cycle with reduced mass

10, 20 °C/min), recording heating and cooling, calculating solid and liquid fractions, the sample Ambient N, 20 ml/min. (Fig. 13) demonstrates a tenth analysis measurement of the fourth sample was heating and cooling, calculating solid fractions with multi-cycle with reduced mass. The sample weight is about 2/3 of the previous measurements (~ 80 mg vs. ~ 120 mg). Compared to sample 3 results, peak heat flows decreased, but the measurement limit still exceeded 20 °C/min. The total temperature window in the plotted range is 540–660 °C. The repeatability of the measurement is less accurate for the lower rates, especially for the solidification of the alpha phase. Inspection of the samples shows a large amount of oxidization.

Figures 14, 15, 16 demonstrate an analysis measurement of the sample was still 10 and 20 °C/min, peaks are smeared, and high values exceed measurement limits.

The two reactions are distinguishable; even at low rates, heating, and cooling peaks are shifted.

The first heating/cooling and first reheat cycles at 0.5 °C/min show some minor deviation, indicating a difference between the initial state and the reheated state of the sample.

Tables 6 and 7 illustrate an analysis measurement of the sample where characteristic temperatures are the onset of the transformation, a breakpoint, and the ending of the transformation. At heating, at 0.5 °C/min curves slightly deviated from the others, as the sample is in the initial state, second heating

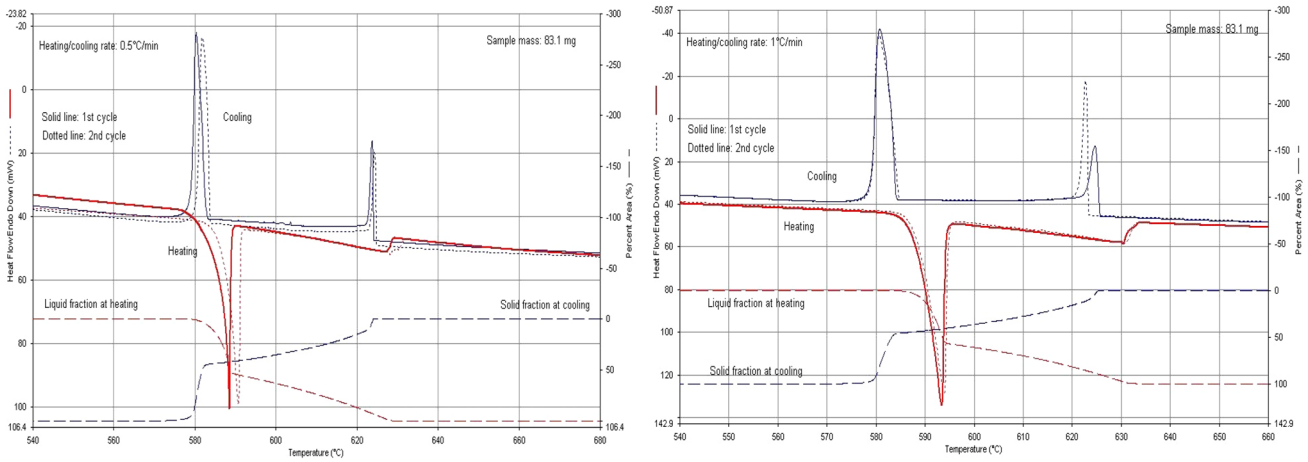

Fig. 14 DSC heating curve of the Al alloy Heating, cooling, and first cycle solid fraction for 0.5 °C/min and 1 °C/min heating rate

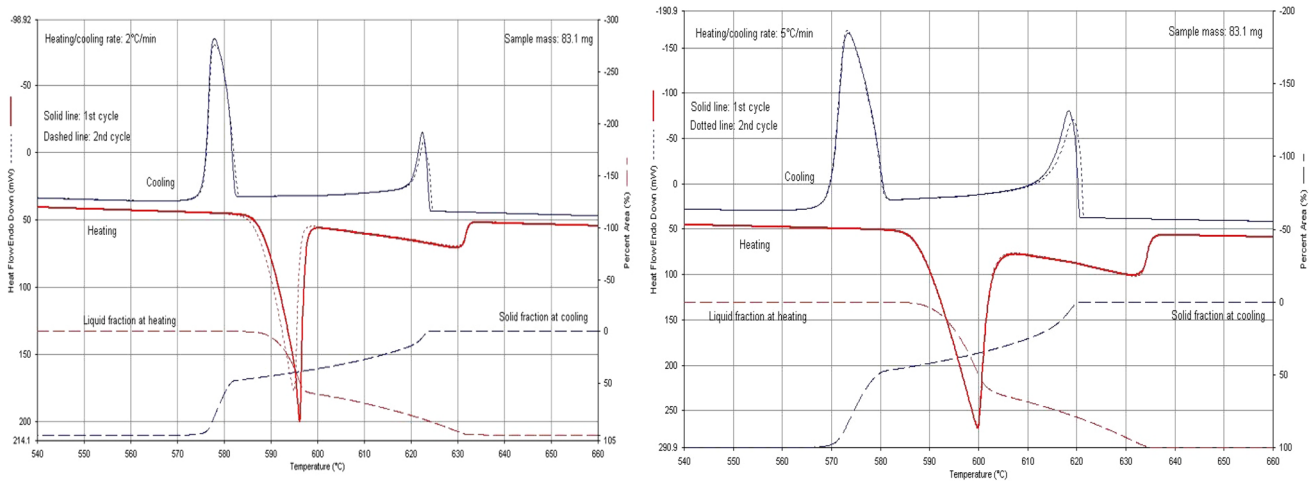

Fig. 15 DSC heating curve of the Al alloy Heating, cooling, and first cycle solid fraction for 2 °C/min and 5 °C/min heating rate

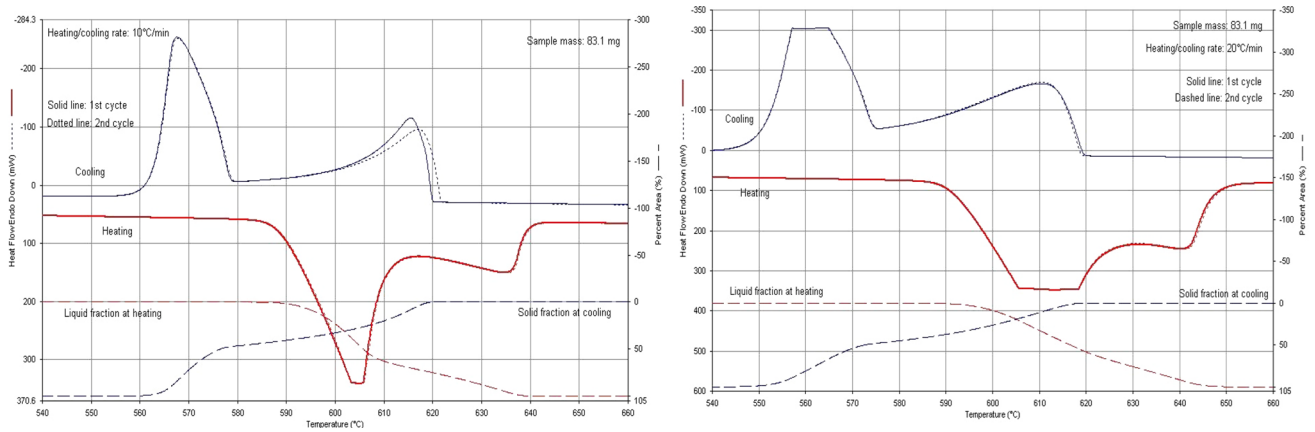

Fig. 16 DSC heating curve of the Al alloy Heating, cooling, and first cycle solid fraction for 10 °C/min and 20 °C/min heating rate

Table 6 Heat rate, solid fraction transient temperatures, energy in transformation extracted, and enthalpy data extracted for heating rates

Heating rate (C/min)	Liquid fraction transient temperatures (°C)			Energy in transformation (mJ)	Enthalpy (mJ/g)
	Onset	Break ($fl = 0.6$)	Ending		
0.5	576	589	629	35,307	427.87
1	582	594	634	34,315	412.93
2	583	596	635	34,136	410.78
5	584	602	634	33,519	403.35
10	583	608	641	32,888*	395.76*
20	586	–	652	31,960*	384.59*

*Heat flow exceeds measurement limits

at 0.5 °C/min shifts the heating curve to the right, and reheated cases show more similarities in their trends.

There is a slight increasing trend in the onset temperature; enthalpy is distinctly larger for the first heating, the similar for 1 and 2 °C/min, maybe slightly decreasing; data at 10 and 20 are not suitable for comparison due to the exceeded measurement limit in heat flow during the eutectic reactions. At cooling, heat flow deviates at 0.5, 1, and 2 °C/min, but transformation temperatures are very similar, while enthalpy shows an increasing trend. All temperatures show a decreasing trend with the rising heating rates; a deviation is seen at 20 C/min due to the exceeded measurement limit; enthalpy is increasing with the increasing cooling rates.

Table 7 Cooling rate, solid fraction transient temperatures, energy in transformation, and enthalpy data extracted data for cooling rates

Cooling rate (°C/min)	Solid fraction transient temperatures (°C)			Energy in transformation (mJ)	Enthalpy (mJ/g)
	Ending	Break ($fs = 0.5$)	Onset		
0.5	573	583	625	30,206	363.48
1	574	583	626	31,956	384.54
2	572	582	624	32,793	394.62
5	567	579	621	32,713	393.65
10	559	576	620	32,865	395.48
20	543	575	619	31,960*	384.59*

*Heat flow exceeds measurement limits

The heating curve of Al alloy recorded rates of heating and cooling, calculating solid and liquid fractions through multi-cycling with even lower mass

The aim of the measurement of the sample was cycling between 500 and 700 °C with different rates (0.5, 1, 2, 5, 10, 20 °C/min), recording heating and cooling, calculating solid and liquid fractions, and the sample Ambient N, 20 ml/min. (Fig. 17) demonstrates a tenth analysis measurement of the fifth sample weight is further reduced to ~ 40 mg (vs. ~ 80 mg and ~ 120 mg). Compared to sample 4 results, peak heat flows further decrease; the measurement limit covers the largest heating/cooling rates (20 °C/min) as well. The total temperature window in the plotted range is 540–660 °C; the repeatability of the thermal cycles is quite accurate. Inspection of the samples shows a large amount of oxidization; it shows that the bottom is melted; the top of the specimen keeps the original structure, and seemingly the top shell is not melted.

Figures 18, 19, 20 demonstrate an analysis measurement of the sample was the two reactions are well distinguishable all over the heating–cooling rates.

The first heating/cooling and first reheat cycles at 0.5 °C/min show some minor deviation, indicating a difference between the initial state and the reheated state of the sample. The next reheating shows good repeatability.

Figure 21 illustrates an analysis measurement of the sample where characteristic temperatures are the onset of the transformation, a breakpoint, and the ending of the transformation. At heating, at 0.5 °C/min, curves slightly deviated from the others, as the sample is in the initial state. Second heating at 0.5 °C/min shifts the heating curve to the right; reheated cases show more similarities in their trends.

There is a slight increasing trend in the onset temperature. Enthalpy is distinctly larger for the first heating, similar for 1 and 2 °C/min, maybe slightly decreasing; data at 10 and 20 are not suitable for comparison due to the exceeded measurement limit in heat flow during the eutectic reactions. At cooling, heat flow deviates at 0.5, 1, and 2 °C/min, but transformation temperatures are very similar, while enthalpy shows an increasing trend. All temperatures show a decreasing trend with the rising heating rates; a deviation is seen at 20 °C/min due to the exceeded measurement limit. Enthalpy is increasing with the increasing cooling rates.

Figure 21 demonstrates an analysis measurement of the sample was latent heat trends vs. the heating/cooling rate;

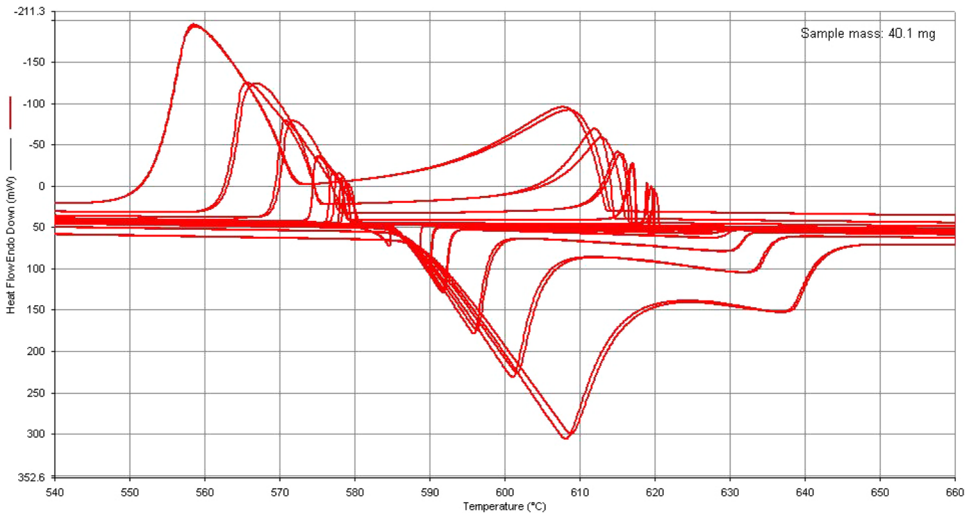

Fig. 17 DSC heating curve of the Al alloy eleventh sample measured heat flow overview, multi-cycle with further reduced mass

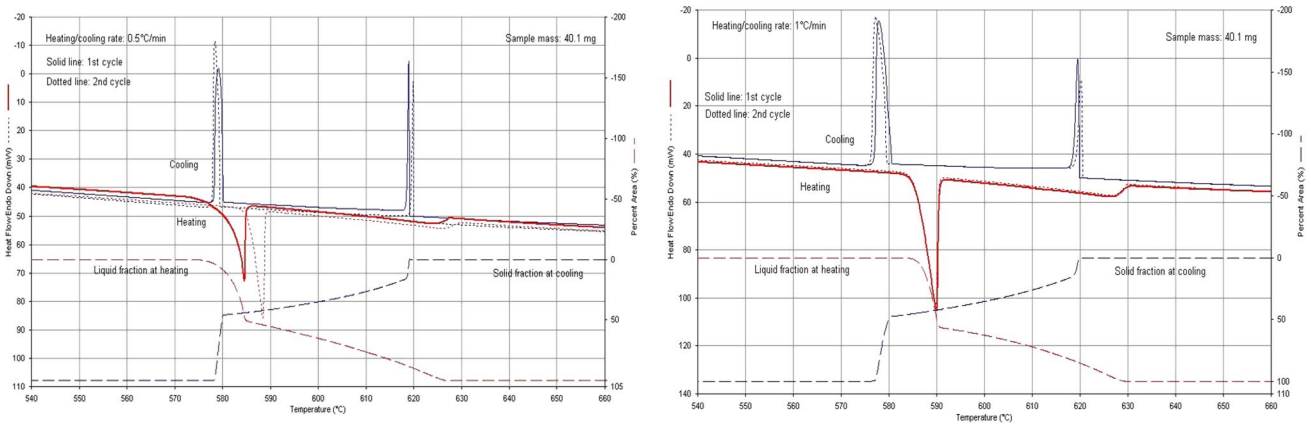

Fig. 18 DSC heating curve of the Al alloy heating, cooling, and solid and liquid fraction for each heating rate for 0.5 °C/min and 1 °C/min heating rate

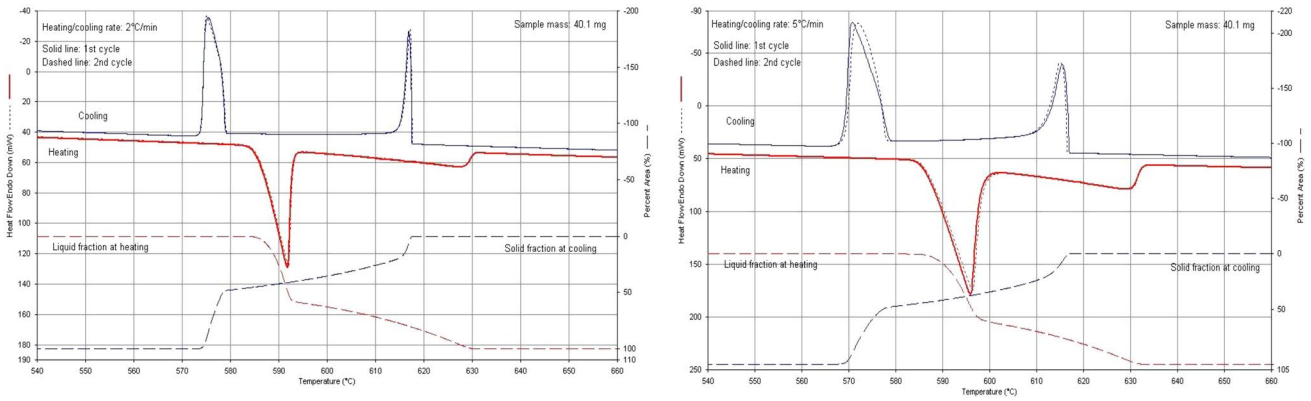

Fig. 19 DSC heating curve of the Al alloy heating, cooling, and solid and liquid fraction for each heating rate for 2 °C/min and 5 °C/min heating rate

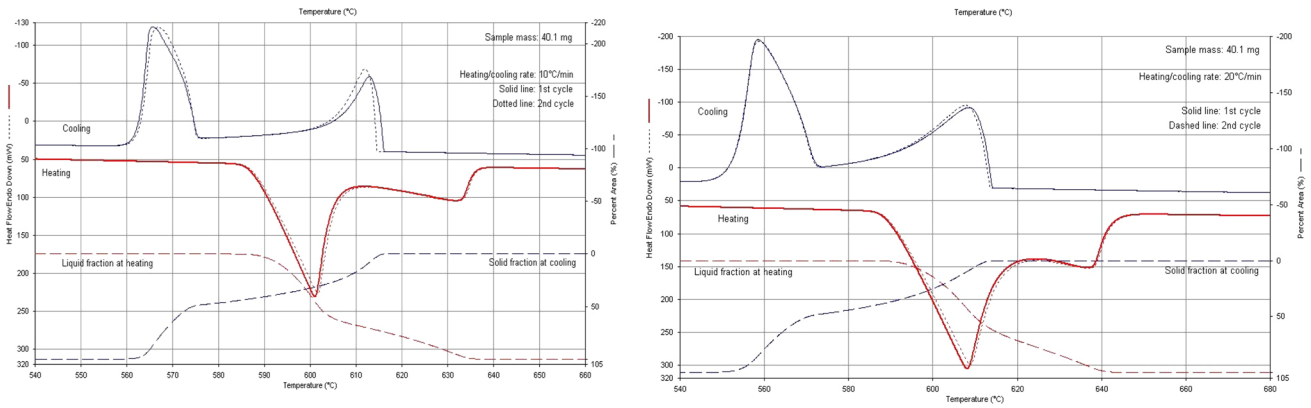

Fig. 20 DSC heating curve of the Al alloy heating, cooling, and solid and liquid fraction for each heating rate for 10 °C/min and 20 °C/min heating rate

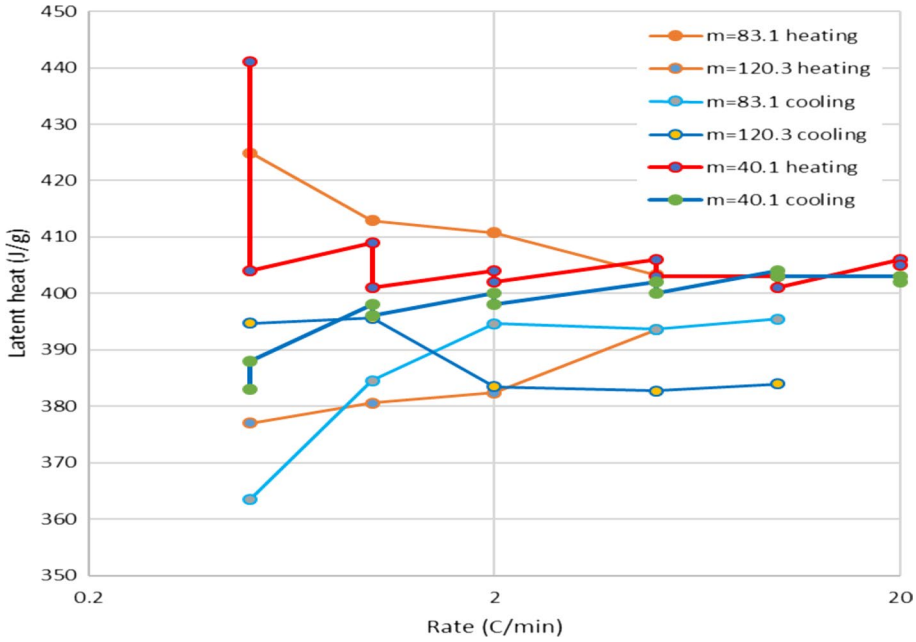

Fig. 21 Latent heat trends vs the heating/cooling rate

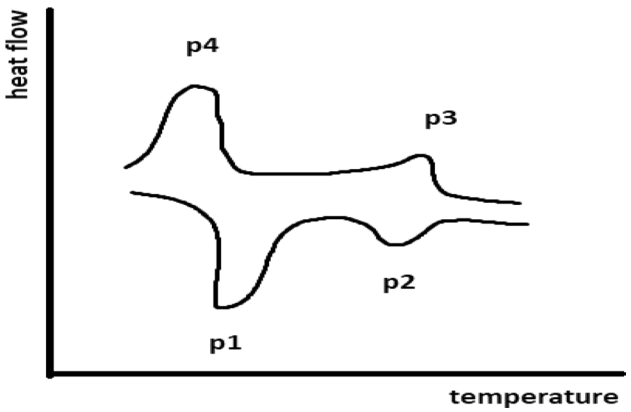

Fig. 22 Characteristic peak temperatures

the data extraction from the last measurement set (Al5, $m = 40.1$ mg) is the most accurate, and it shows reliable trends. Enthalpy for first heating and cooling deviates from the subsequent thermal cycles. In the subsequent thermal cycles, reproducibility is good. Enthalpies in heating with increasing rates are decreasing, enthalpies in cooling with rising rates are growing, and enthalpies are asymptotic towards a value a bit higher than 400 J/g (~ latent heat for pure Al = 396 J/g). Latent heat for AlSi7 in the literature is at 480–500 J/g.

Figures 22, 23 demonstrate an eleventh measurement of the sample each peak moves with a different speed concerning the heating/cooling rates. At 3 heating and cooling, peaks would be located at identical temperatures at the intersection of the corresponding lines in the diagram.

The intersection of eutectic peaks in (Fig. 23) (p1 heating, and p4 cooling) would be at a heating/cooling rate of 0.17 °C/min, and the intersection of alpha peaks (p2 heating, and p3 cooling) would be at a heating/cooling rate of 0.39 °C/min.

Conclusions

This study demonstrated the DSC analysis and microstructures of Al-Si EN AB-42000 rheocasting semi-solid alloy. The following key findings were obtained:

1. High heating rates smear the two peaks in the mushy zone, while low rates result in slow measurements. Smaller sample weights and slower rates are preferable.
2. The shape of the *fs* curve, exact composition, and contaminant-less reference composition must be analysed to understand complex behaviours, such as pseudo-eutectic behaviours. The thermal sensitivity of compositions is also crucial.
3. Heat flow decreases with a decreased sample weight, but the measurement limit is still exceeded at high heating/cooling rates (20 °C/min) for the eutectic reaction.
4. The peaks are higher for the eutectic reaction, with enthalpies in the range of 360–430 mJ/g, but difficult to conclude trends in heating versus cooling and low-mass versus higher-mass samples.
5. The temperature range for the non-equilibrium transformation of eutectic is more confined, while alpha transformation is more spread, and reactions overlap with increasing rates.

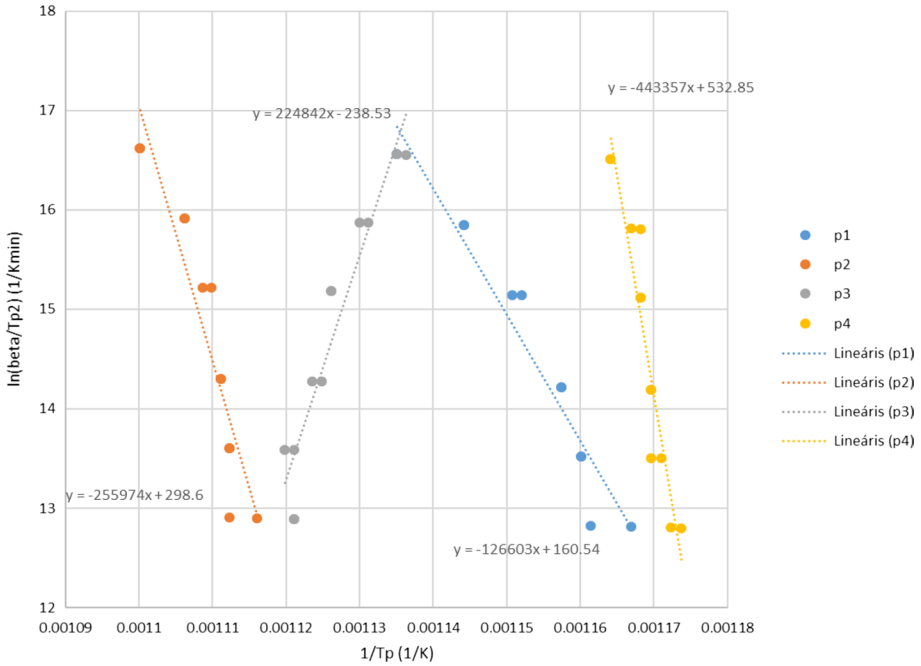

Fig. 23 Kissinger plot of the peaks

6. Industrial needs, like shorter test durations, often determine rate choices.
7. Further research should examine various rates for a complete thermal behaviour view.

Funding Open access funding provided by Óbuda University.

Declarations

Conflict of interest The authors declare that they have no conflict of interest.

Ethical approval This article does not contain any studies with human participants or animals performed by any of the authors.

Informed consent Formal consent is not required for this type of study.

References

1. Janovszky D et al (2022) Amorphous alloys and differential scanning calorimetry (DSC). J Anal Calorim Therm. https://doi.org/10.1007/s10973-021-11054-0
2. Höhne GWH, Hemminger WF, Flammersheim HJ, Höhne GWH, Hemminger WF, Flammersheim HJ (2003) Applications of differential scanning calorimetry. Springer, Berlin Heidelberg. https://doi.org/10.1007/978-3-662-03302-9
3. Murray JL, McAlister AJ (1984) The Al-Si (aluminum-silicon) system. Bull Alloy Phase Diag 5(1):74–84. https://doi.org/10.3390/ma10060676
4. Chen Z, Liu K, Elgallad E, Breton F, Chen X-G (2020) Differential scanning calorimetry fingerprints of various heat-treatment tempers of different aluminum alloys. Metals 10(6):763. https://doi.org/10.3390/met10060763
5. Wu Y, Ye L, Jia Y, Ling LIU, Zhang X (2014) Precipitation kinetics of 2519A aluminum alloy based on aging curves and DSC analysis. Trans Nonferrous Met Soc China 24(10):3076–3083. https://doi.org/10.1016/S1003-6326(14)63445-2
6. Chang CST, Banhart J (2011) Low-temperature differential scanning calorimetry of an Al–Mg–Si alloy. Metall Mater Trans A 42:1960–1964. https://doi.org/10.1007/s11661-010-0596-5
7. Starink MJ (2004) Analysis of aluminium based alloys by calorimetry: quantitative analysis of reactions and reaction kinetics. Int Mater Rev 49(3–4):191–226. https://doi.org/10.1016/j.tca.2009.01.027
8. Payandeh M (2015) Rheocasting of aluminium alloys: slurry formation, microstructure, and properties. Jönköping Univ School Eng. https://doi.org/10.13140/RG.2.1.1464.7122
9. Thanabumrungkul S, Janudom S, Burapa R, Dulyapraphant P, Wannasin J (2010) Industrial development of gas induced semi-solid process. Trans Nonferrous Met Soc China 20:s1016–s1021. https://doi.org/10.4028/www.scientific.net/AMR.881-883.1597
10. Kirkwood DH, Suéry M, Kapranos P, Atkinson HV, Young KP (2010) Semi-solid processing of alloys, vol 124. Springer, Cham. https://doi.org/10.1007/978-3-642-00706-4

11. Gupta AK, Marois PH, Lloyd DJ (1996) Study of the precipitation kinetics in a 6000 series automotive sheet material. Mater Sci Forum. https://doi.org/10.1007/s11663-006-9003-4
12. Zhuang L, De Haan R, Bottema J, Lahaye CTW, De Smet P (2000) Improvement in bake hardening response of Al–Si–Mg alloys. Mater Sci Forum. https://doi.org/10.4028/www.scientific.net/MSF.331-337.1309
13. Arockiasamy A, German R, Wang P, Horstemeyer M, Suri P, Park S (2010) DSC analysis of Al6061 aluminum alloy powder by rapid solidification: effect of additives. J Therm Anal Calorim 100(1):361–366. https://doi.org/10.1007/s10973-009-0587-1
14. Hung Y et al (2023) Isodimorphic crystallization and thermally-induced crystal transitions in poly (octamethylene-ran-decamethylene carbonate): critical role of comonomer defects. Polymer 274:125903. https://doi.org/10.1016/j.polymer.2023.125903
15. An X et al (2023) Microstructure and solidification behaviour of CuNiSiAl eutectic multi-principal element alloy. Mater Sci Technol. https://doi.org/10.1080/02670836.2023.2210917
16. Kundu A, Biswas P, Sahu M, Patel D, Mallik A, Das S (2023) Effect of electromagnetic flow direction on grain refinement of Al 2024 alloy. JOM 75:1–19
17. Das P (2023) Effect of melt treatment on microstructure evolution and coarsening mechanism of A356 Al alloy during cooling slope rheoprocessing. Metall Mater Trans B 54(3):1383–1407
18. Birol Y (2009) Solid fraction analysis with DSC in semi-solid metal processing. J Alloys Compd 486(1–2):173–177. https://doi.org/10.1016/j.jallcom.2009.06.165
19. Modigell M, Koke J (1999) Time-dependent rheological properties of semi-solid metal alloys. Mech Time-Dependent Mater 3:15–30. https://doi.org/10.3390/met8040245
20. Blanco A, Azpilgain Z, Lozares J, Kapranos P, Hurtado I (2010) Rheological characterization of A201 aluminum alloy. Trans Nonferrous Met Soc China 20(9):1638–1642. https://doi.org/10.1016/S1003-6326(09)60351-4
21. Pezda J (2009) Effect of modifying process on mechanical properties of EN AB-42000 silumin cast into sand moulds. Arch Found Eng 9(4):187–190
22. Pezda J (2011) Effect of T6 heat treatment on mechanical properties and microstructure of EN AB-42000 alloy modified with strontium. Archiv Found Eng 11:169–174
23. Pezda J (2012) T6 heat treatment of hypo-eutectic silumins in aspect of improvement of Rm tensile strength. Arch Foundry Eng 12(2s):49–52
24. Kolb GK-H, Scheiber S, Antrekowitsch H, Uggowitzer PJ, Pöschmann D, Pogatscher S (2016) Differential scanning calorimetry and thermodynamic predictions—a comparative study of Al–Zn–Mg–Cu alloys. Metals 6(8):180. https://doi.org/10.3390/met6080180
25. De Mori A, Timelli G, Fabrizi A, Berto F (2021) Influence of Cu content on the microstructure and high-temperature tensile and fatigue properties of secondary AlSi7Mg0. 3VZr alloys. Mater Sci Eng A 816:141310. https://doi.org/10.1016/j.msea.2021.141310
26. Dutkiewicz J, Atkinson HV, Lityńska-Dobrzyńska L, Czeppe T, Modigell M (2013) Characterization of semi-solid processing of aluminium alloy 7075 with Sc and Zr additions. Mater Sci Eng A 580:362–373. https://doi.org/10.1016/j.msea.2013.04.078
27. Birol Y (2010) Internal cooling process to prepare aluminium rheocasting feedstock. Int J Cast Met Res 23(1):55–59. https://doi.org/10.1179/174313309X455302
28. Atkinson HV, Burke K, Vaneetveld G (2008) Recrystallisation in the semi-solid state in 7075 aluminium alloy. Mater Sci Eng A 490(1–2):266–276. https://doi.org/10.1016/j.msea.2008.01.057
29. Göpel W, Reinhardt G, Rösch M (2000) Trends in the development of solid state amperometric and potentiometric high temperature sensors. Solid State Ionics 136:519–531. https://doi.org/10.1016/S0167-2738(00)00410-0
30. Midson SP (2015) Industrial applications for aluminum semi-solid castings. Solid State Phenom 217:487–495. https://doi.org/10.3390/met8030181
31. Nkoua C, Josse C, Proietti A, Basséguy R, Blanc C (2023) Corrosion behaviour of the microbially modified surface of 5083 aluminium alloy. Corros Sci 210:110812. https://doi.org/10.1016/j.corsci.2022.110812
32. Trudonoshyn O (2020) Design of Al–Mg–Si–Mn alloys with Zn, Cr and Sc additions with unique strengthening response. PQDT-Global
33. Abdulrahman KM, Gonda V, Réger M (2018) Comparison of the techniques to produce non-dendritic feedstocks for thixoforming. Bánki Közlemények 1(2):57–61
34. Heugue P, Larouche D, Breton F, Massinon D, Martinez R, Chen XG (2019) Precipitation kinetics and evaluation of the interfacial mobility of precipitates in an $AlSi7Cu_{3.5}Mg_{0.15}$ cast alloy with Zr and V additions. Metals 9(7):777. https://doi.org/10.3390/met9070777
35. Grieshop S (2014) Comparison of the corrosion behavior of high strength aluminum alloys after exposure to ASTM B117 environment. http://hdl.handle.net/1811/60362
36. Vedani M, Angella G, Bassani P, Ripamonti D, Tuissi A (2007) DSC analysis of strengthening precipitates in ultrafine Al–Mg–Si alloys. J Therm Anal Calorim 87:277–284. https://doi.org/10.1016/S1003-6326(14)63543-3
37. Das P (2023) Microstructure evolution during Rheoprocessing of A356 Al alloy using cooling slope. Int J Met 17(3):1982–2001